ELSEVIER

Polymer 42 (2001) 9929–9940

polymer

www.elsevier.com/locate/polymer

Nylon 6 nanocomposites: the effect of matrix molecular weight

T.D. Fornes, P.J. Yoon, H. Keskkula, D.R. Paul*

Department of Chemical Engineering and Texas Materials Institute, Center for Polymer Research, The University of Texas at Austin, Austin, TX 78712-1062, USA

Received 30 April 2001; received in revised form 24 June 2001; accepted 26 July 2001

Abstract

Organoclay nanocomposites based on three different molecular weight grades of nylon 6 were prepared by melt processing using a twin screw extruder. Mechanical properties, transmission electron microscopy, wide-angle X-ray diffraction, and rheological measurements were used to characterize the three types of composites. Tensile modulus and yield strength were found to increase with increasing concentration of clay, while elongation at break decreased. Izod impact strength was relatively independent of clay content for the higher molecular weight composites, but slightly decreased with increasing clay content for the lowest molecular weight polyamide. In general, nanocomposites based on the higher molecular weight polyamides yielded superior composite properties, having higher degrees of clay exfoliation, higher stiffness and yield strength values, and marginal loss of ductility as compared to nanocomposites based on the low molecular weight polyamide. Differences in properties between the three types of composites were attributed to differences in melt rheology. Capillary and dynamic parallel plate data revealed sizeable differences in the levels of shear stress between each nanocomposites system. A mechanism for exfoliation during melt mixing is outlined.

Keywords: Nanocomposites; Matrix molecular weight; Montmorillonite

1. Introduction

Polymer layered silicate nanocomposites have become an important area of polymer composite research. The work by the Toyoto group [1–5] provided the stimulus for subsequent theoretical and applied research over the last decade. Numerous studies have demonstrated that only a few percent of layered silicate can lead to a wide array of property enhancements, e.g. increased stiffness and strength [6–9], improved solvent and UV resistance [10–12], enhanced gas barrier properties [13–15], greater dimensional stability [6,7,16], and superior flame retardancy [17,18].

Despite the recent progress in polymer nanocomposite technology, there are many fundamental questions that have not been answered. For example, how do changes in polymer crystalline structure induced by the clay affect overall composite properties? How does one tailor organoclay chemistry to achieve high degrees of exfoliation reproducibly for a given polymer system? How do process parameters and fabrication affect composite properties? Although some research is in progress that addresses such issues [19,20], a focused effort is needed to develop a better understanding of how superior nanocomposites are formed.

At present, there are four principal methods for producing exfoliated nanocomposites; (1) in situ polymerization [2,5,10,21], (2) emulsion polymerization [22,23], (3) sol–gel templating [24,25], and (4) melt compounding [7,26,27]. A majority of current nanocomposite research has focused on nanocomposites derived from polymerization-based techniques, i.e. the first three techniques listed above. However, little information is available concerning the formation of nanocomposites via melt compounding.

Early work by Giannelis et al. [26,28,29] revealed that intercalation of polymer chains into the galleries of an organoclay can occur spontaneously by heating a mixture of polymer and silicate clay powder above the polymer glass transition or melt temperature. Once sufficient polymer mobility is achieved, chains diffuse into the host silicate clay galleries, thereby producing an expanded polymer–silicate layer structure. Intercalation is greatly enhanced by maximizing the number of polymer host interactions through appropriate selection of organically modified silicate [26].

Vaia et al. have stated that intercalation can be improved through the aid of conventional processing techniques [30,31]. Indeed, nanocomposites have been formed using a variety of shear devices (e.g. extruders, mixers, ultrasonicators,

* Corresponding author. Tel.: +1-512-471-5392; fax: +1-512-471-0542.
E-mail address: drp@che.utexas.edu (D.R. Paul).

0032-3861/01/$ - see front matter
PII: S0032-3861(01)00552-3

Table 1
Materials used in this study

Material [designation used here]	Supplier designation	Specification	Supplier
Nylon 6 [LMW]	Capron 8202	$\bar{M}_n = 16\,400$,[a] MFI = 23.0	Honeywell (formerly AlliedSignal)
Nylon 6 [MMW]	Capron B73WP	$\bar{M}_n = 22\,000$,[a] MFI = 4.5	Honeywell (formerly AlliedSignal)
Nylon 6 [HMW]	Capron B135WP	$\bar{M}_n = 29\,300$,[a] MFI = 1.2	Honeywell (formerly AlliedSignal)
Organoclay $[(HE)_2M_1R_1]$[b]	Bis(hydroxyethyl)-(methyl)-rapeseed quaternary ammonium organoclay	Organic loading = 95 mequiv./100 g clay, organic content = 34.6 wt%	Southern Clay Products

[a] $\bar{M}_n$ determined via intrinsic viscosity using *m*-cresol at 25°C [35].

[b] The substituents on the quaternary ammonium compound used to form the organoclay are identified in this shorthand notation where R = rapeseed, HE = hydroxyethyl, M = methyl. Rapeseed is a natural product composed predominantly of unsaturated C_{22} alkyl chains (45%).

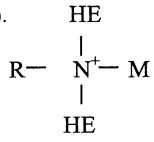

etc.). Of these melt processing techniques, twin screw extrusion has proven to be most effective for the exfoliation and dispersion of silicate layers. Owing to the combination of shear and good polymer–organoclay affinity, twin screw extrusion leads to composite properties comparable to those produced by in situ techniques [32]. The advantages of forming nanocomposites by melt processing are quite appealing. Melt processing is environmentally sound since no solvents are required. It shifts nanocomposite production downstream, thereby giving end-use manufacturers many degrees of freedom with regard to final product specifications (e.g. selection of polymer grade, choice of organoclay, level of reinforcement, etc.). At the same time, melt processing minimizes capital costs due to its compatibility with existing processes.

Recent studies have demonstrated that melt processing conditions play a key role in achieving high levels of exfoliation [32–34]. Results from these studies indicate that an optimum balance between residence time and level of shear is required to facilitate the exfoliation and dispersion of layered silicates. In addition, proper choice of organoclay chemistry is critical.

The purpose of this paper is to examine the effect of nylon 6 molecular weight on the properties of nanocomposites formed from organically modified layered silicates by melt processing. Mechanical properties are reported for composites based on three different molecular weight grades of nylon 6. These materials were characterized by transmission electron microscopy, X-ray diffraction, and rheological measurements. This paper is the first of a series that will explore organoclay structure–property relationships, thermo-mechanical behavior, and orientation effects in injection molded specimens.

2. Experimental

2.1. Materials

The materials used in this study are described in Table 1. Commercial grades of nylon 6 were chosen that span the range of melt viscosities commonly used in commercial injection molding and extrusion applications. The three materials represent low, medium, and high molecular weight grades and will be referred to as LMW, MMW, and HMW. The organoclay was formed by a cation exchange reaction between sodium montmorillonite (CEC = 92 mequiv./100 g clay) and bis(hydroxyethyl)-(methyl)-rapeseed quaternary ammonium chloride, designated here as $(HE)_2M_1R_1$, and was obtained from Southern Clay Products. Thermal stability properties of this organoclay have been reported by Cho et al. [32]. All data below are reported in terms of the weight percent montmorillonite (MMT) in the composite rather than the amount of organoclay, since the silicate is the reinforcing component.

2.2. Melt processing

Melt blended composites were prepared using a Haake, co-rotating, intermeshing twin screw extruder (Length = 305 mm, $L/D = 10$). The screws are of modular design with varying degrees of mixing along the length of screws. The screw modules were configured to achieve an optimum level of shearing and residence time as reported earlier [32–34]. Compounding was carried out at a barrel temperature of 240°C, a screw speed of 280 rpm, and a feed rate of 980 g/h. Prior to each melt processing step, all polyamide containing materials were dried in a vacuum oven at 80°C for a minimum of 16 h. Residence time distributions, presented in Fig. 1, were determined on each virgin polyamide according to procedures outlined by Shon et al. [36]. To ensure an accurate assessment of the level of MMT in each composite blend, dried pellets were placed in a furnace at 900°C for 45 min and the amount of residue was determined. The results were corrected for loss of structural water [37,38]. The percent MMT in the final nanocomposite was calculated from

$$\%\mathrm{MMT} = \%\mathrm{MMT}_{ash}/0.935 \quad (1)$$

where $\%\mathrm{MMT}_{ash}$ is the mass after incineration relative to the

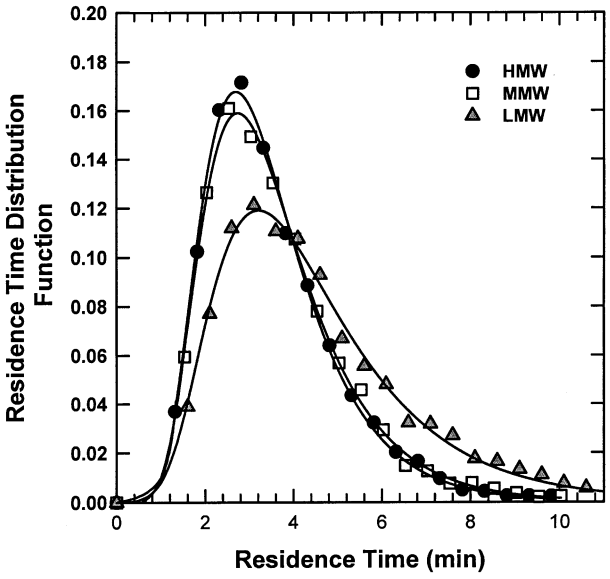

Fig. 1. Residence time distribution curves for the twin screw extruder at the die exit for pure nylon 6 materials: LMW, MMW, and HMW.

original nanocomposite mass. The actual percentage of 'oganoclay' in the final nanocomposite, $\%\text{organoclay}_{NC}$, is determined by the following relation:

$$\%\text{organoclay}_{NC} = \%\text{MMT}_{ash}\left[\frac{\text{OC}}{100-\text{OC}} - 0.065\right] \quad (2)$$

where OC is the % organic content in the organoclay as listed in Table 1. The quantities 0.935 and 0.065 in these equations account for the loss of structural water during incineration.

Extruded composite pellets were injection molded into standard tensile (ASTMD638, Type I) and Izod specimens (ASTM D256) using an Arburg Allrounder 305-210-700 injection molding machine. Test specimens were prepared using a barrel temperature of 260°C, mold temperature of 80°C, injection pressure of 70 bar, and a holding pressure of 35 bar. After molding, the specimens were immediately sealed in a polyethylene bag and placed in a vacuum desiccator for a minimum of 24 h prior to mechanical testing.

2.3. Mechanical testing

Tensile tests were conducted according to ASTM D628 using an Instron model 1137 testing machine. Modulus and yield strength were determined at a crosshead speed of 0.51 cm/min, while elongation at break data were collected at both 0.51 and 5.1 cm/min. An extensometer was used to accurately determine Young's modulus and yield strength. Elongation at break values were calculated from crosshead travel and an effective gauge length (9.04 cm) as described by Lindsey [39]. Notched Izod impact tests were performed at room temperature using a TMI Izod tester (6.8 J hammer and 3.5 m/s impact velocity) according to ASTM D256. Property values reported here represent an average of the results for tests run on six specimens. Standard deviations were typically of the order of 4% for modulus, 1% for yield strength, and 15% for Izod impact strength. Elongation at break values tended to be more variable with standard deviations typically in the range 5–25% of the value reported.

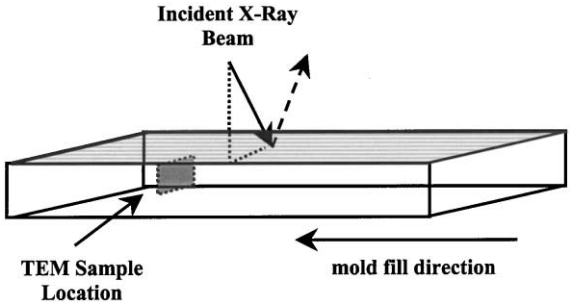

Fig. 2. Illustration of incident X-ray path and TEM sampling location.

2.4. Transmission electron microsocpy (TEM)

Samples for TEM analysis were taken from a central cross-section of an Izod bar, as depicted in Fig. 2. The sample region was located normal to the flow direction at a distance of 2.5 cm from the far end of a 13 cm Izod bar and half-way between the top and bottom surfaces of the bar. Ultra-thin sections ranging from 50 to 60 nm in thickness were cryogenically cut with a diamond knife at a temperature of −40°C using a Reichert–Jung Ultracut E microtome. Sections were collected on 300 mesh copper TEM grids and subsequently dried with filter paper. The sections were examined by TEM using a JEOL 2010 TEM with a LaB_6 filament operating at an accelerating voltage of 200 kV. The resulting images were analyzed for average particle size, size distribution, and extent of exfoliation. TEM images were printed on $20.3 \times 25.4\ \text{cm}^2$ photographic paper to ensure an accurate image analysis. A transparent plastic sheet was placed over the print and dispersed platelets and/or agglomerates were traced. The resulting transparency was scanned and subsequently analyzed using an image analysis software package (NIH® Image software, Scion Image). Specific magnifications were chosen to include a substantial number of platelets/agglomerates in order to improve the statistical validity of the analysis.

2.5. Wide-angle X-ray diffraction (WAXD)

WAXD was conducted using a Sintag XDS 2000 diffractometer. WAXD scans were obtained in reflection mode using an incident X-ray wavelength of 1.542 Å at a scan rate of 1.0 deg/min. X-ray analysis was performed on Izod bars except for the organoclay, which was in powder form. The Izod specimens were oriented such that the incident beam reflected off the transverse face, as depicted in Fig. 2.

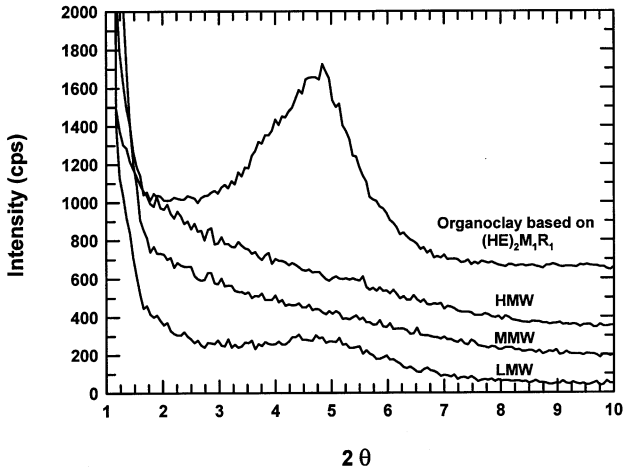

Fig. 3. WAXD patterns for $(HE)_2M_1R_1$ organoclay and $(HE)_2M_1R_1$ organoclay nanocomposites based on LWM, MMW, and HMW nylon 6 matrices containing ~1.5 wt% montmorillonite. The curves are vertically offset for clarity.

2.6. Rheology

Dynamic rheological measurements were performed using a Rheometric Scientific rotational rheometer (Advanced Rheometric Expansion System). Rheological properties of the virgin polyamides and the $(HE)_2M_1R_1$ based organoclay nanocomposites were measured using 25 mm diameter parallel plates in oscillatory shear mode. Dynamic storage modulus, G', and dynamic loss modulus, G'', were recorded as functions of angular frequency, ω, at 240°C. The frequency test range was from 0.01 to 100 rad/s. Rheological test specimens were taken from tensile bars, which were dried for 16 h in vacuum at 80°C prior to each experiment. Specimens were placed between the preheated parallel plates and were allowed to equilibrate for 15 min prior to each frequency sweep run. A fixed strain of 0.1 was used to ensure that measurements were taken within the linear viscoelastic range of the materials. Experiments were conducted under a nitrogen atmosphere in order to prevent oxidative degradation of the specimens. The temperature control was accurate to within ±1°C.

Steady shear viscosities, η, were measured at 240°C using an Instron Capillary Rheometer equipped with a long capillary die having a diameter of 1.58 mm and a length of 40 mm. Capillary data were corrected using the Rabinowitsch–Mooney relationship in order to obtain true shear viscosities. Details of this analysis are described elsewhere [40].

3. Characterization

Fig. 3 compares X-ray diffraction patterns for the pristine organoclay, derived from $(HE)_2M_1R_1$, and the nanocomposites based on the three nylon 6 materials, LMW, MMW, and HMW, having an approximate montmorillonite concentration of 1.5 wt% MMT. The organoclay pattern reveals a broad intense peak around $2\theta = 5°$, corresponding to a basal spacing of 18.0 Å. The MMW and HMW X-ray patterns do not show a characteristic basal reflection, which is indicative of an exfoliated structure. However, the LMW composite pattern reveals a low, broad shallow peak around $5^{\circ\circ}$ of 2θ, which is characteristic of pure $(HE)_2M_1R_1$ organoclay basal spacings. At $2\theta < 5°$, the intensity falls with decreasing angle until approximately 3°, where the intensity begins to rise. The LMW X-ray results suggest that the system is of mixed form having regions of intercalated clay and regions of exfoliated clay platelets. These trends fro the HMW, MMW, and LMW composites were consistent at each concentration of MMT. The above X-ray results suggest that melt rheology may play a significant role in the formation of exfoliated structures. It should be noted that the X-ray intensity was found to increase with increasing molecular weight of the nylon 6 matrix at a given MMT concentration and with MMT concentration for each molecular weight. Additional work is in progress to explore this behavior in more detail.

TEM photomicrographs of the $(HE)_2M_1R_1$ organoclay nylon 6 composites, shown in Fig. 4, provide a better representation of the composite structure. The HMW and MMW nanocomposite images, Fig. 4(a) and (b), reveal well exfoliated structures, in agreement with the WAXD results. Image analysis data, presented in Table 2, provide a quantitative comparison between the different composites. The mean TEM particle density, which is the average number of particles per μm^2, is a measure of the extent of exfoliation. A particle can be defined as one dispersed platelet or as an agglomerate of plates, as depicted in Fig. 5. These TEM particle densities were divided by the weight percent MMT concentration to obtain the quantity designed here as specific particle density. The specific particle densities at ~3.0 wt% MMT for the HMW and MMW composites are 83.1 and 67.4, respectively, indicating a larger extent of platelet exfoliation for the HMW composite. The specific particle density values are also consistent with the observed average number of platelets per stack. The HMW composite, having an average of 1.3 platelets per stack, consists predominantly of individual platelets with a certain fraction of doublets, triplets, and higher aggregates. The MMW composites contain a higher fraction of multiple platelet stacks, thus yielding a higher average number platelets per stack of 1.5.

The LMW composite photomicrograph reveals partial exfoliation with areas containing exfoliated platelets and areas of intercalated structures. The extent of exfoliation for the 3.0 wt% MMT-LMW composite is significantly lower at a specific density of 30.7 particles per μm^2, in comparison to the HMW and MMW results. The lower level of exfoliation is also evident in the average number of platelets per stack, 2.4. In addition, the LMW composites have larger platelet lengths than the higher molecular weight composites. There are several possible reasons for

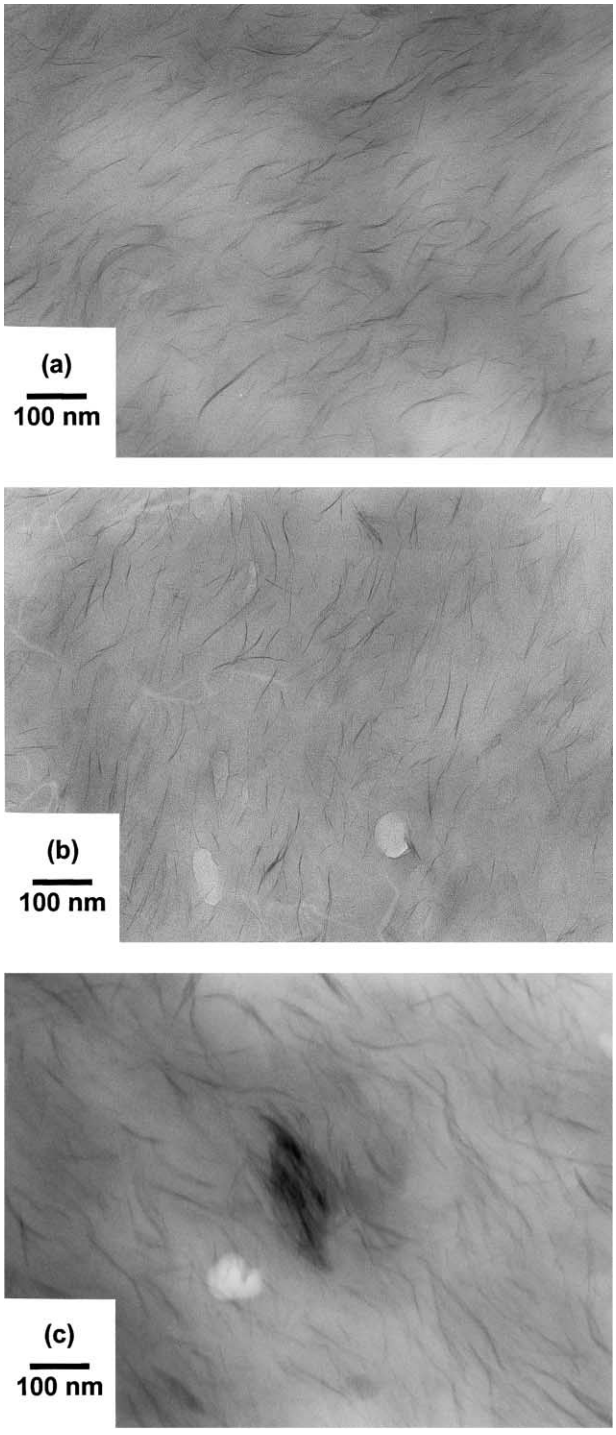

Fig. 4. TEM micrographs of melt compounded nanocomposites containing ~3.0 wt% montmorillonite based on (a) HMW, (b) MMW, and (c) LMW nylon 6.

the relationship between molecular weight and particle length. The shorter lengths for the higher molecular weight polyamides may be a result of attrition due to the higher melt viscosities of the polyamide matrix; this is commonly seen in other systems such as glass fiber composites. Melt viscosity differences between the LMW, MMW, and HMW matrices may also play another role in determining the

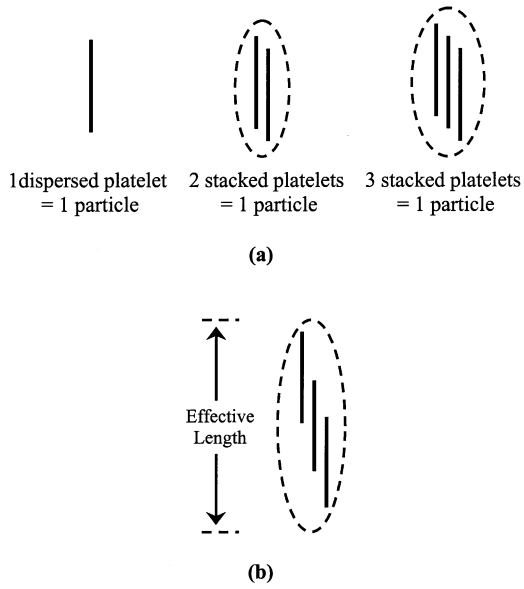

Fig. 5. TEM analysis methodology for (a) counting particles and (b) measuring effective particle length.

observed length of the clay particles. The higher molecular weight systems, due to their higher melt viscosities, transfer more stress or energy to achieve separation of platelets. However, a low molecular matrix imparts low shear stresses on the agglomerates, which may skew the stack of platelets rather than separate them, as depicted in Fig. 6. Such skewed stacks would appear larger.

4. Mechanical properties

Fig. 7 shows the effect of montmorillonite concentration and nylon 6 molecular weight on the modulus of nanocomposites formed from $(HE)_2M_1R_1$ organoclay. The addition of the organoclay leads to substantial improvement in stiffness for the composites based on each of the three polyamides. Interestingly, the stiffness increases with increasing nylon 6 molecular weight at any given montmorillonite concentration even thought the moduli of the neat polyamides are all quite similar. Table 3 summarizes the moduli and other mechanical properties of the virgin materials and selected $(HE)_2M_1R_1$ organoclay/nylon 6 nanocomposites. The slightly larger modulus of 2.82 GPa for LMW may be the

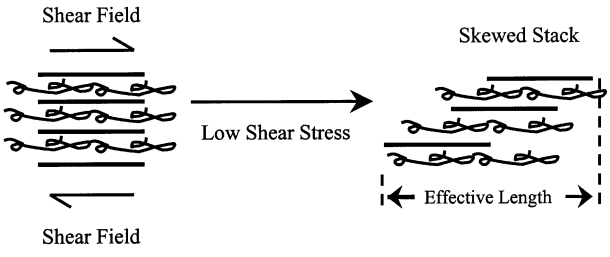

Fig. 6. A possible mechanism for the cause of larger effective particle sizes for the LMW nanocomposites.

Table 2
TEM analysis results for nylon 6 $(HE)_2M_1R_1$ organoclay nanocomposites

Nylon 6 $(HE)_2M_1R_1$ organoclay nanocomposites	Platelet length (nm)	Average number of platelets/stack	TEM particle density[a] (μm^{-2})	Specific particle density[b] (μm^{-2})
LMW				
1.6 wt% MMT	110	~2.2	41	25.6
3.0 wt% MMT	122	~2.4	92	30.7
MMW				
1.4 wt% MMT	78	~1.5	80	57.1
3.1 wt% MMT	82	~1.5	209	67.4
HMW				
1.6 wt% MMT	75	~1.4	97	60.6
2.9 wt% MMT	77	~1.3	241	83.1

[a] The TEM particle density is the average number of montmorillonite particles per μm^2.
[b] The specific particle density is TEM particle density divided by the MMT concentration.

result of a higher degree of crystallinity due to faster crystallization kinetics during the cooling of the specimen during injection molding. Despite these small differences in base materials, the higher molecular weight matrices consistently yield higher levels of nanocomposite stiffness.

Similar trends with respect to level of organoclay content and molecular weight are evident in the yield strength results. Fig. 8 shows the dependence of yield strength on montmorillonite content and molecular weight. Yield strength increases with the concentration of montmorillonite. However, there are notable differences in the level of strength improvement for the different molecular weights even though the yield strengths for the pure polyamides are nearly identical. The HMW and MMW based materials show a steady increase in strength with concentration of clay, while the LMW composites show a less pronounced effect. The differences in strength improvement with respect to molecular weight are most prominent at the highest clay concentration. The increase in strength relative to the virgin matrix for the HMW composite is nearly double that of the LMW composite.

The relationship between montmorillonite content and elongation at break for the different matrices is shown in Fig. 9 for two rates of extension. Fig. 9(a) shows that the virgin polyamides are very ductile at a test rate of 0.51 cm/min. Increasing the clay content leads to a sacrifice in ductility. However, the HMW and MMW based composites maintain reasonable levels of ductility at MMT concentrations as high as 3.5 wt%. Elongation at break for the LMW based composites decreases rapidly at low MMT concentrations around 1 wt% MMT. The larger reduction in the LMW system may be attributed to the presence of unexfoliated aggregates, as seen in the TEM results described earlier. At the higher testing speed of 5.1 cm/min, shown in Fig. 9(b), similar trends are seen, but the absolute levels of elongation at break values are significantly lower. Interestingly, the strain at break for LWM composites is relatively independent of rate of extension, similar to what has been reported for glass fiber reinforced composites [32]. Table 3 shows that strain at yield also decreases with clay loading. Even at the highest clay concentration, the HMW composite exhibits ductile fracture (i.e. specimens elongate beyond the

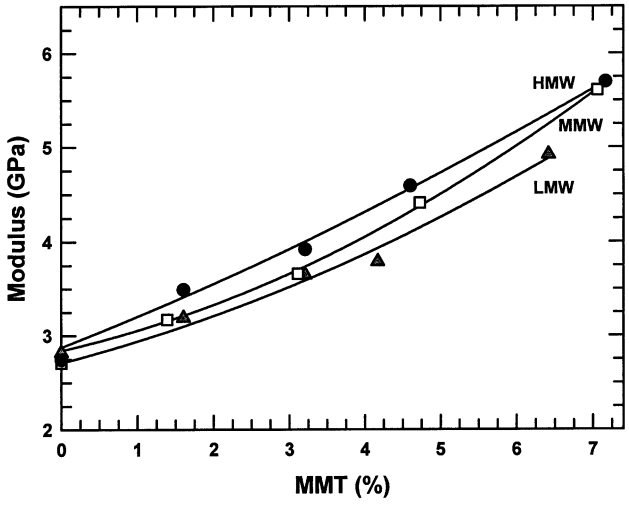

Fig. 7. Effect of montmorillonite content on tensile modulus for LMW, MMW, and HMW based composites.

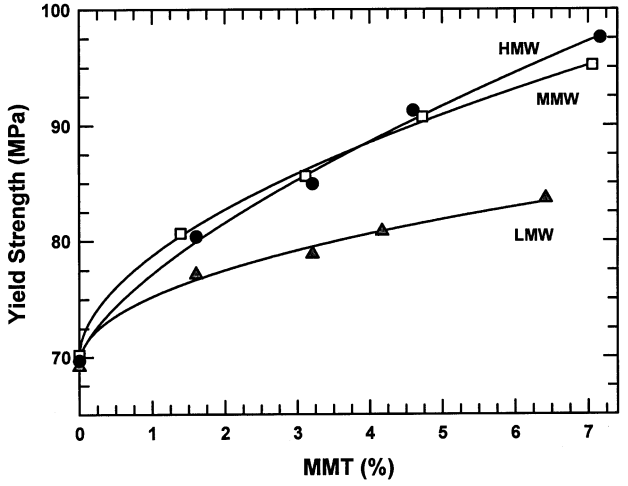

Fig. 8. Effect of montmorillonite content on yield strength for LMW, MMW and HMW based composites.

Table 3
Select mechanical properties for nylon 6 $(HE)_2M_1R_1$ organoclay nanocomposites

Nylon 6 $(HE)_2M_1R_1$ organoclay nanocomposites	Modulus (GPa)	Yield strength (MPa)	Strain at yield point[a] (%)	Elongation at break (%)		Izod impact strength (J/m)
				Crosshead speed 0.51 cm/min	Crosshead speed 5.1 cm/min	
LMW						
0.0 wt% MMT	2.82	69.2	4.0	232	28	36.0
3.2 wt% MMT	3.65	78.9	3.5	12	11	32.3
6.4 wt% MMT	4.92	83.6	2.2	2.4	4.8	32.0
MMW						
0.0 wt% MMT	2.71	70.2	4.0	269	101	39.3
3.1 wt% MMT	3.66	85.6	3.5	81	18	38.3
7.1 wt% MMT	5.61	95.2	2.4	2.5	5	39.3
HMW						
0.0 wt% MMT	2.75	69.7	4.0	3.4	129	43.9
3.2 wt% MMT	3.92	84.9	3.3	119	27	44.7
7.2 wt% MMT	5.70	97.6	2.6	4.1	6.1	46.2

[a] Strain measured during modulus and yield strength testing using a cross speed of 0.51 cm/min.

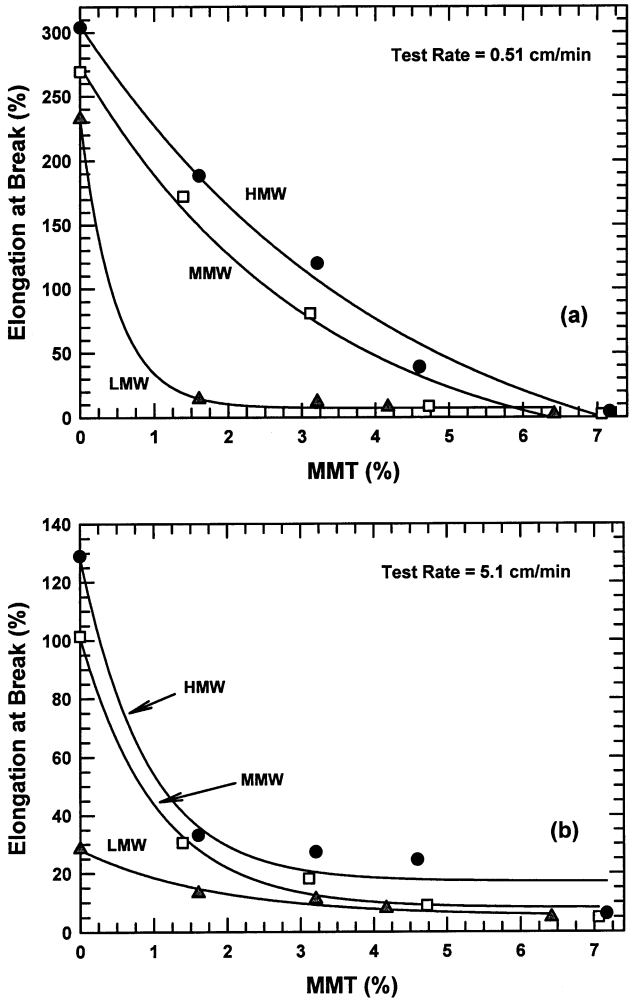

Fig. 9. Effect of montmorillonite content on elongation at break for LMW, MMW, and HMW based composites at a crosshead speed of (a) 0.51 cm/min and (b) 5.1 cm/min.

yield point and exhibit necking). On the other hand, the LMW and MMW composites fracture in a brittle manner at the highest clay concentration.

The notched Izod impact strength, shown in Fig. 10, is relatively independent of clay concentration for the HMW and MMW composites, but gradually decreases for the LMW composites. At any given $(HE)_2M_1R_1$ organoclay concentration, impact strength increases with increasing molecular weight. This trend primarily reflects differences in the polyamide fracture energy. These Izod values and the above tensile properties are comparable to, and in some cases, better than previously reported for nylon 6 nanocomposites [6,7,27,32].

The above results show that the properties of the nanocomposites formed by melt compounding are highly dependent upon the molecular weight of the nylon 6. These relationships between composite properties and

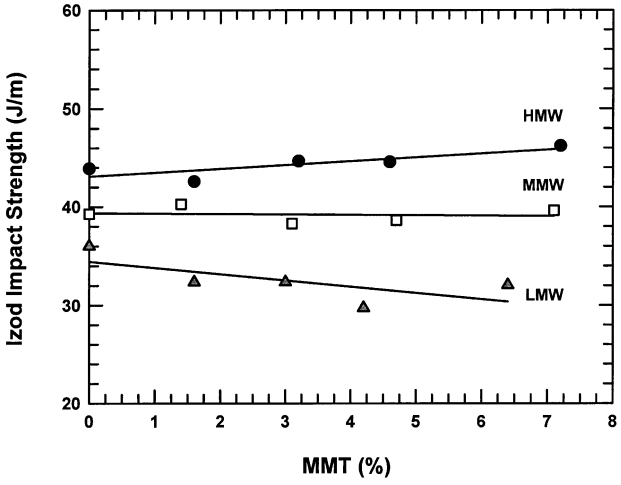

Fig. 10. Effect of montmorillonite content on Izod impact strength for LMW, MMW, and HMW based composites.

matrix molecular weight are somewhat inconsistent with what might be anticipated from prior theoretical and fundamental studies dealing with how polymer molecular weight affects the intercalation and exfoliation of organoclay. Theoretical modeling of polymer–clay phase behavior by Lyatskaya suggests that formation of exfoliated structures requires use of polymers with low degrees of polymerization and minimal affinity for the clay surface [41]. In a different study, Vaia and Giannelis compared the intercalation kinetics of polystyrenes of different molecular weights into the galleries of a fluorohectorite-based organoclay. They found that kinetics of intercalation at 160°C rapidly decreased with increasing polystyrene molecular weight [30]. Of course, the underling mechanisms involved in these studies differ from those operative in this work. These studies employ static experimental conditions, while melt compounding involves high levels of shear and mixing. The result presented in this paper suggest that melt rheology plays a key role in the formation of exfoliated nanocomposites and that molecular weight dependent diffusion processes, although possibly important, do not limit the formation of intercalated and exfoliated structures. Indeed, Vaia and Giannelis showed that formation of intercalated hybrids proceeded rapidly when extruding mixtures of organoclay with a high molecular weight polystryene ($\bar{M}_w = 300\,000$) at 250°C [30]. It is informative to examine more carefully the rheological differences between the base nylon 6 materials and the nanocomposites formed from them.

5. Rheological behavior

Due to the necessity for understanding the influence of various shear environments on polymer nanocomposite systems, the rheological behavior of nanocomposites have received considerable attention over the past several years [32,42,43]. Notably, Krishnamoorti and Giannelis found that the viscoelastic behavior of in situ derived polycaprolactone nanocomposites containing a high silicate concentration was greatly dependent on the level of strain amplitude and ultimately silicate orientation [42,43]. They observed a large reduction in shear modulus G' and loss modulus G'' when applying a large-amplitude oscillatory strain in comparison to a small strain. This reduction was attributed to alignment of silicate layers parallel to the applied shear. More recently, Cho and Paul [32] observed that melt compounded nylon 6 nanocomposites showed lower steady-shear viscosities than that of pristine polymer in regions of high shear when using a capillary rheometer. They suggested that thermal degradation of the polymer matrix during melt blending could be one of several possible mechanisms for the less viscous nanocomposites and that these types of shear dependent phenomena should be examined more carefully. This section seeks to explain the viscoelastic behavior of the current nylon 6 nanocomposites over a wide range of frequencies or shear rates using two different shearing techniques.

Fig. 11 shows logarithmic plots of complex viscosity, $|\eta^*|$, versus angular frequency, ω, at 240°C for pure nylon 6 and $(HE)_2M_1R_1$ organoclay nanocomposites based on (a) HMW, (b) MMW, and (c) LMW obtained using the parallel plate oscillating rheometer. Fig. 11 also gives plots of steady-state shear viscosity η versus shear rate $\dot{\gamma}$ obtained using a capillary rheometer. The nanocomposites contain ~3.0 wt% MMT. Several trends in Fig. 11 should be addressed. First, the complex viscosity and steady-shear viscosity increase with increasing molecular weight for the pure polyamides and in the nanocomposites, as expected. Second, there are significant differences in the low frequency oscillatory data between the three nanocomposites. The HMW nanocomposite exhibits solid-like non-Newtonian behavior, gradually increasing with decreasing frequency. In contrast, the low frequency response for the MMW based nanocomposite reveals Newtonian-like behavior, having a nearly constant complex viscosity at frequencies less than 0.2 rad/s. The LMW composite exhibits a more pronounced Newtonian response with a Newtonian plateau beginning at 5 rad/s. This particular trend is more clearly represented in plot of G' versus ω due to the extreme sensitivity of G' to morphological state, as seen in Fig. 12. The terminal zone slope of 1.5 for the pure LMW polyamide deviates from the monodispersed, terminal zone slope of 2.0, indicating polydispersed behavior. It should be noted that the terminal slopes for MMW and HMW homopolymers are approximately the same as the LMW homopolymer. The HMW nanocomposite exhibits a lower terminal zone slope compared to the MMW and LMW based composites. The differences in slopes may be attributed to differences in extent of exfoliation. A larger extent of exfoliation will lead to more solid-like behavior due to the increased number of particle–polymer interactions. However, the underlying differences in matrix molecular weight between the three systems must not be completely ruled out, since the onset of Newtonian behavior occurs at lower frequencies for the higher molecular weight pristine polyamides. Interestingly, the trends seen here for these melt compounded nanocomposites are quite similar to those observed for in situ polymerized nylon 6 nanocomposites, as reported by Krishnamoorti and Giannelis [43].

The steady shear capillary data shows a trend with respect to polyamide molecular weight. Steady shear viscosities for the HMW and MMW based nanocomposites are lower than their pure matrix viscosities in the shear rate ranges of $\dot{\gamma} = 6$–$200\ s^{-1}$ and 7–$200\ s^{-1}$, respectively, as seen in Fig. 11(a) and (b). On the other hand, the LMW nanocomposite viscosities are higher than pure LMW nylon 6 in the range of $\dot{\gamma} = 7$–$80\ s^{-1}$. The lower shear viscosities for HMW and MMW nanocomposites, compared to their pristine matrices, may be attributed to higher degrees of exfoliation, and smaller platelet sizes.

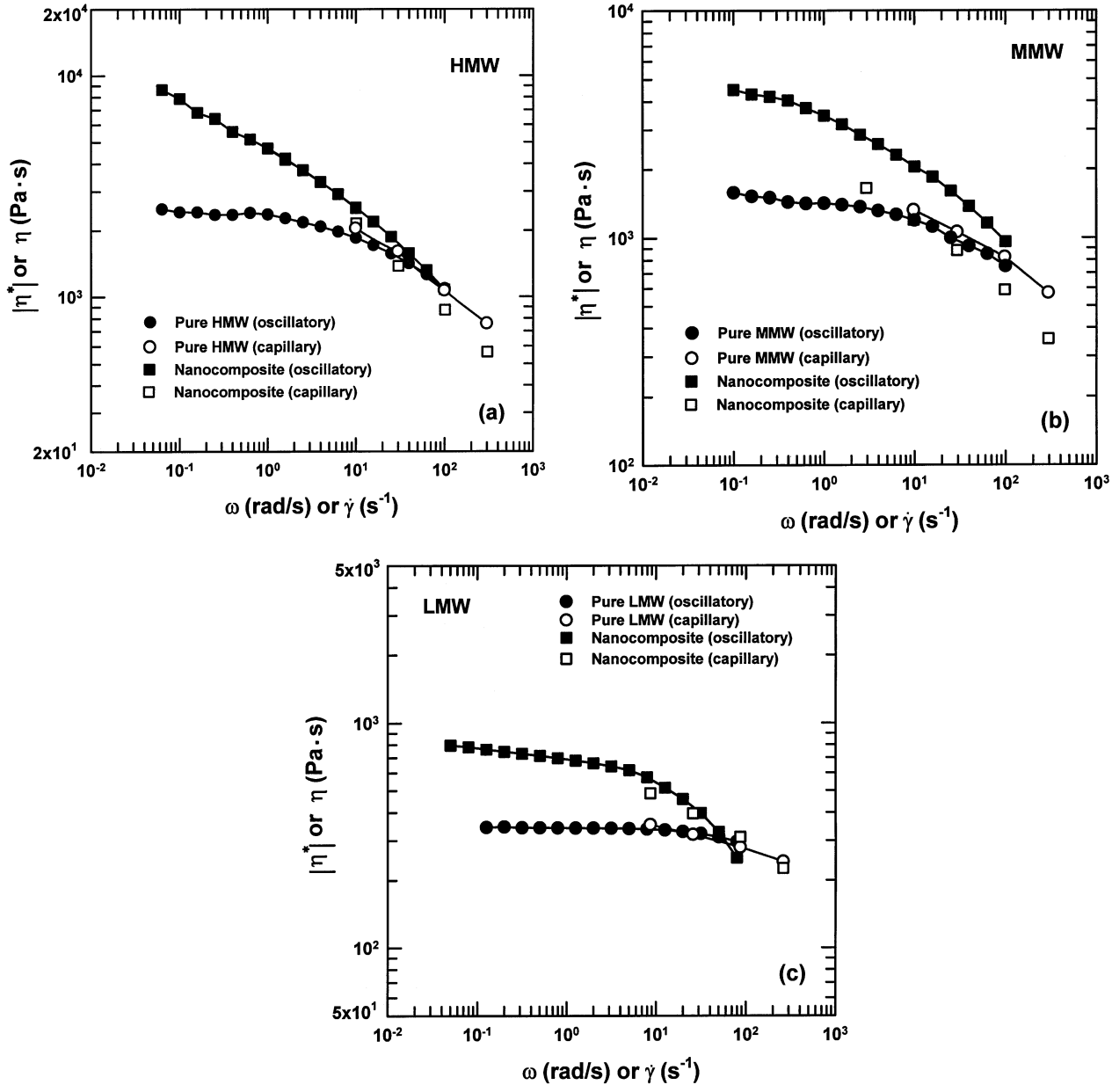

Fig. 11. Complex viscosity versus frequency from a dynamic parallel plate rheometer (solid points) and steady shear viscosity versus shear rate from a capillary rheometer (open points) at 240°C for (a) pure HMW and its $(HE)_2M_1R_1$ organoclay nanocomposite, (b) pure MMW and its $(HE)_2M_1R_1$ organoclay nanocomposite. The nanocomposites contain ~3.0 wt% MMT.

Platelets on the nanometer scale can be easily aligned during shear flow, particularly for matrices imparting high shear stresses. The LMW nanocomposites contain a relatively large percent of non-exfoliated silicate particles which are most difficult to align, particularly with lower inherent shear stress levels. The LMW nanocomposite system behaves similar to conventional filled systems, thus giving higher viscosities than pure LMW nylon 6. However, the molecular weight degradation of the matrix cannot be ruled out, as mentioned by Cho and Paul [36]. Preliminary intrinsic viscosity data on these materials reveal a measurable decrease in matrix molecular weight, particularly for the higher molecular weight polyamide composites. This work will be further explored in a future publication.

An additional point should be addressed concerning Fig. 11. The Cox–Merz rule [44], which states that $|\eta^*|(\omega) = \eta(\dot{\gamma})$ when $\omega = \dot{\gamma}$, is valid for the pure polyamides but fails for the nanocomposite systems. Such failure is not uncommon and has been reported for liquid crystalline polymers [45], polymer–polymer blends [46], particle filled polymers [47], fiber-reinforced polymers [48], micro-separated block copolymers [49], and even polymer nanocomposites [43]. There are various

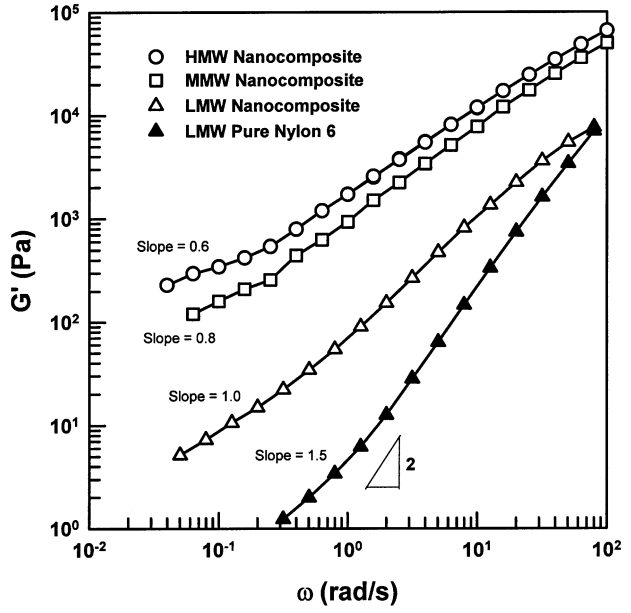

Fig. 12. Influence of frequency on shear storage modulus for pure LMW, and for LMW, MMW and HMW based nanocomposites.

factors identified in these studies that may contribute to the break down of the Cox–Merz rule. For example, Han et al. found that flow geometry affected rheological behavior of blends of poly(methyl methacrylate) and polystyrene which exhibited different morphological states by the cone-and-plate rheometer and capillary rheometer [46]. Nakajima et al. observed in carbon black/rubber composites that shear viscosity obtained by capillary rheometry was significantly lower than the corresponding dynamic quantity due to strain hardening with extension in dynamic measurements [47]. Bailey et al. reported that the Cox–Merz rule was not obeyed in glass fiber reinforced nylon 6 and polypropylene due to dramatic changes in fiber orientation from shearing in a capillary [48]. It is reasonable to expect that the nanocomposites behave similarly to glass fibers with regard Cox–Merz rule deviations, in that the clay platelets orient in the direction of flow. Deviations from the Cox–Merz rule for nanocomposites have also been observed in polystyrene–polyisoprene block copolymer nanocomposites as determined by Krishnamoorthi et al. [50]. However, in order to completely explain the failure of the Cox–Merz rule in the nanocomposite, explicit details of the morphological states of the clay platelets and polymer molecules in the different flow geometries are needed, which is beyond the scope of this paper.

Overall, it is imperative to emphasize the relative differences in melt viscosity between these three systems. Over the range of frequencies and shear rates tested, the melt viscosity varies from approximately 350 Pa s for pure LMW, 1700–550 Pa s for pure MMW, and 2200–750 Pa s for pure HMW. From these shear rate ranges, corresponding shear stress, τ, ranges can be calculated

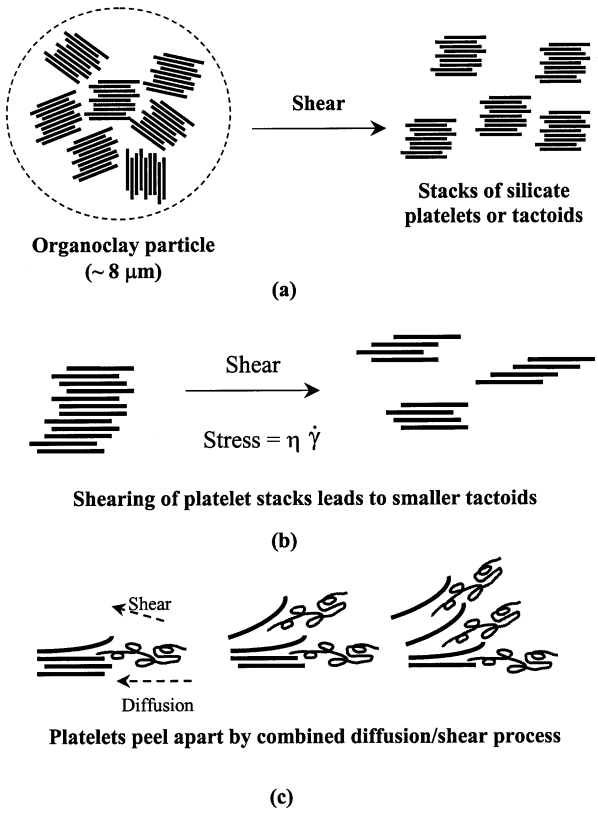

Fig. 13. Stepwise mechanism of clay platelet exfoliation in the melt compounding of nanocomposites: (a) organoclay particle breakup, (b) clay tactoid breakup, and (c) platelet exfoliation.

from,

$$\tau = \eta\dot{\gamma} \tag{3}$$

The resulting shear stresses exerted by the pure polyamides during processing are approximately 35 Pa to 75 kPa for LMW, 170 Pa to 165 kPa for MMW, and 220 Pa to 225 kPa for HMW. Therefore, during mixing, the level of stress exerted on the organoclay by the LMW melt are significantly lower than those developed by the MMW and HMW melts. The stress levels imparted by the HMW polyamide are between three and six times that of the LMW system over the range of shear rates tested. It believed that high levels of shear stress aid in the breakup of clay particles and ultimately improve clay platelet exfoliation. Fig. 13 schematically suggests the various roles that shear stress may play during the melt compounding of nanocomposites. Initially, the stress should help breakup large organoclay particles into dispersed stacks of silicate tactoids, as depicted in Fig. 13(a). Further down the extruder, transfer of the stress from the molten polymer to the silicate tactoids is believed to shear them into smaller stacks of silicate platelets as illustrated in Fig. 13(b). Ultimately, individual platelets peel apart through a combination of shear and diffusion of polymer chains in the organoclay gallery, as suggested in Fig. 13(c). There is ample microscopy evidence to show that

individual aluminosilicate layers are quite flexible. Therefore, the platelet on the top or bottom of a stack is able to bend away from others in the stack as the polymer chains seek to wet or make contact with the organoclay surface. This layer-by-layer peeling mechanism appears to greatly reduce the conventionally envisioned resistance to intercalation resulting form polymer chain confinement in the galleries between the platelets that are not able to bend as would be true in the mild-layers of a tactoid stack [51]. The model suggested in Fig. 13 was proposed recently on the basis of an extensive study of processing nanocomposites [34]. The role of polymer molecular weight demonstrated here is believed to stem from the fact that a high melt viscosity exerts a greater stress on the tactoids and that the stress shears the taller stacks into shorter ones. The final step in exfoliation involves peeling the platelets of the stacks one by one; and this takes time and requires the matrix polymer to have sufficient affinity for the clay surface to cause spontaneous wetting. To some extent, this can be controlled by the nature of the organic treatment given to the clay. The shorter the stacks can be made by stress, the less time needed for peeling the layers away. For a fixed residence time, a higher stress should then translate into a higher degree of exfoliation. There may be, however, some critical stress needed to reduce stack size, and the LMW nylon 6 melt may not generate stresses of this critical level. It should be noted that according to this model, stress alone cannot achieve exfoliation when the matrix polymer lacks sufficient compatibility with the organoclay.

6. Conclusion

Nanocomposites based on three different molecular weight grades on nylon 6 (low, medium, and high) were prepared using a co-rotating twin screw extruder. WAXD and TEM results collectively reveal a mixed structure for the LMW based nanocomposites, having regions of intercalated and exfoliated clay platelets, while the MMW and HMW composites revealed well exfoliated structures. Qualitative TEM observations were supported by a quantitative analysis of high magnification TEM images. The average number of platelets per stack was shown to decrease with increasing nylon 6 molecular weight. The TEM particle density, which is the average number of silicate particles per μm^2, increased with increasing molecular weight, thereby revealing larger extents of clay platelet exfoliation for the nanocomposites in the order HMW > MMW > LWM composites. Mechanical properties were consistent with the morphological structure found via WAXD and TEM. Tensile properties revealed superior performance for the higher molecular weight nylon 6 composites, particularly those based on HMW. The HMW based nanocomposites have the highest moduli, yield strengths, and elongation at break.

Dynamic and steady shear capillary experiments were performed on the pure polyamides and polyamide nanocomposites over a large range of frequencies and shear rates. Low frequency viscosity data obtained via parallel plate experiments revealed solid-like, non-Newtonian behavior for the HMW nanocomposites, while MMW and LMW composites exhibited Newtonian plateaus at low frequencies. The trend may be associated with differences in levels of clay platelet exfoliation between the three nanocomposites. Capillary data revealed lower viscosities for the MMW and HMW nanocomposites relative to their pure matrix values. This phenomenon may be the result of higher clay platelet alignment, smaller particle sizes, and/or matrix molecular weight degradation. The melt viscosity and consequently the shear stress, increase with increasing nylon 6 molecular weight. The higher shear stress is believed to be the major contributor to exceptional exfoliation of clay platelets in the higher molecular weight matrix.

Acknowledgements

This work was supported by the Texas Advanced Technology Program under grant number 003658-0067. The authors would like to thank Southern Clay Products Inc. for providing clay materials, WAXD analyses, and for many helpful discussions. We also thank Prof. Peter F. Green for use of the parallel plate rheometer.

References

[1] Okada A, Fukushima Y, Kawasumi M, Inagaki S, Usuki A, Sugiyami S, Kurauchi T, Kamigaito O. US Patent Number 4739007, 1988 (assigned to Toyoto Motor Co., Japan).
[2] Kawasumi M, Kohzaki M, Kojima Y, Okada A, Kamigaito O. United States Patent Number 4810734; 1989 (assigned to Toyoto Motor Co., Japan).
[3] Fukushima Y, Inagaki S. J Incl Phenom 1987;5:473–82.
[4] Kojima Y, Usuki A, Kawasumi M, Okada A, Kurauchi T, Kamigaito OJ. Polym Sci, Part A: Polym Chem 1993;31:983–6.
[5] Usuki A, Kojima Y, Kawasumi M, Okada A, Fukushima Y, Kurauchi T, Kamigaito O. J Mater Res 1993;8(5):1179–84.
[6] Usuki A, Koiwai A, Kojima Y, Kawasumi M, Okada A, Kurauchi T, Kamigaito O. J Appl Polym Sci 1995;55:119–23.
[7] Liu L, Qi Z, Zhu X. J Appl Polym Sci 1999;71:1133–8.
[8] Lan T, Pinnavaia TJ. Chem Mater 1994;6:2216–9.
[9] Wang Z, Pinnavaia TJ. Chem Mater 1998;10:3769–71.
[10] Kojima Y, Usuki A, Kawasumi M, Okada A, Kurauchi T, Kamigaito O. J Appl Polym Sci 1993;49:1259–64.
[11] Huang J-C, Zhu Z-k, Yin J, Qian X-f, Sun Y-Y. Polymer 2001;42(3):873–7.
[12] Lincoln DM, Vaia RA, Sanders JH, Philips SD, Cutler JN, Cerbus CA. Polym Mater: Sci Engng 2000;82:230–1.
[13] Messesmith PB, Giannelis EP. J Polym Sci, Part A: Polym Chem 1995;33:1047–57.
[14] Yano K, Usuki A, Okada A, Kurauchi T, Kamigaito O. J Polym Sci, Part A: Polym Chem 1993;31:2493–8.
[15] Barbee RB, Matayabas Jr. JC, Gilmer JW. PCT Int Appl WO 99/02593 (assigned to Eastman Chemical Company).
[16] Gu A, Chang F-C. J Appl Polym Sci 2001;79:289–94.
[17] Gilman JW. Appl Clay Sci 1999;15:31–49.

[18] Vaia RA, Price G, Ruth PN, Nguyen HT, Lichtenhan J. Appl Clay Sci 1999;15:67–92.
[19] Gilman JW, Morgan AB, Harris Jr. RH, Trulove PC, DeLong HC, Sutto TE. Polym Mater: Sci Engng 2000;83:59–60.
[20] Lincoln DM, Vaia RA, Wang Z-G, Hsiao BS. Polymer 2001;42:1621–31.
[21] Weimer MW, Chen H, Giannelis EP, Sogah DY. J Am Chem Soc 1999;121:1615–6.
[22] Lee DC, Jang LW. J Appl Polym Sci 1996;61:1117–22.
[23] Lee DC, Jang LW. J Appl Polym Sci 1998;68:1997–2005.
[24] Gregar KC, Winans RE, Botto RE. US Patent 5308808, 1994 (assigned to US Department Energy).
[25] Carrado KA, Xu L. Chem Mater 1998;10:1440–5.
[26] Vaia RA, Ishii H, Giannelis EP. Chem Mater 1993;5:1694–6.
[27] Christiani BR, Maxfield M. United States Patent Number 5747560, 1998 (assigned to AlliedSignal Inc).
[28] Mehrotra V, Giannelis EP. Res Soc Symp Proc 1990:171.
[29] Giannelis EP, Mehrotra V, Tse O, Vaia RA, Sung T-C. Mater Res Soc Symp Proc 1992;249:547–58.
[30] Vaia RA, Jandt KD, Kramer EJ, Giannelis EP. Macromolecules 1995;28:8080–5.
[31] Vaia RA, Jandt KD, Kramer EJ, Giannelis EP. Chem Mater 1996;8:2628–35.
[32] Cho JW, Paul DR. Polymer 2001;42(3):1083–94.
[33] Dennis HR, Hunter DL, Chang D, Kim S, White JL, Cho JW, Paul DR. SPE Antec Tech Pap 2000:428–33.
[34] Dennis HR, Hunter DL, Chang D, Kim S, White JL, Cho JW, Paul DR. Polymer 2001;42:9513.
[35] Oshniski AJ, Keskkula H, Paul DR. Polymer 1996;37(22):4891–907.
[36] Shon K, Chang D, White JL. Int Polym Process 1999;1:44–50.
[37] van Olphen H. An introduction to clay colloid chemistry. 2nd ed. New York: Wiley, 1977. Chapter 5.
[38] Hunter D, Knudsen B. Southern clay products, personal communication.
[39] Lindsey C. MS Thesis. The University of Texas at Austin, 1979.
[40] Han CD. Rheology in polymer processing. New York: Academic Press, 1976.
[41] Lyatskaya Y, Balazs AC. Macromolecules 1998;31:6676–80.
[42] Krishnamoorti R, Vaia R, Giannelis EP. Chem Mater 1996;8:1728–34.
[43] Krishnamoorti R, Giannelis EP. Macromolecules 1997;30:4097–102.
[44] Cox WP, Merz EH. J Polym Sci 1958;28:619.
[45] Kim SS, Han CD. Polymer 1994;35:93.
[46] Han JH, Feng CC, Li DJ, Han CD. Polymer 1995;36:2451.
[47] Nakajima N, Bowerman HH, Collins WA. J Appl Polym Sci 1977;21:3063.
[48] Bailey RS, Bellamy AM, Groves DJ, Stocks DM, Young RC. Theor Appl Rheol 1992;2:838.
[49] Yoon PJ. PhD Dissertation. University of Akron, 1999.
[50] Krishnamoorti R, Ren J, Silva AS. J Chem Phys 2001;114(11):4968–73.
[51] Vaia RA, Giannelis EP. Macromolecules 1997;30:7990–9.